Structural instability and charge modulations in the kagome superconductor AV_3Sb_5

Zijin Ye,[1] Aiyun Luo,[1] Jia-Xin Yin,[2] M. Zahid Hasan,[2] and Gang Xu[1,*]

[1]*Wuhan National High Magnetic Field Center and School of Physics, Huazhong University of Science and Technology, Wuhan 430074, China*

[2]*Laboratory for Topological Quantum Matter and Advanced Spectroscopy (B7), Department of Physics, Princeton University, Princeton, New Jersey 08544, USA*

(Received 17 November 2021; revised 7 April 2022; accepted 31 May 2022; published 14 June 2022)

Recently, both charge density wave (CDW) and superconductivity have been observed in the kagome compounds AV_3Sb_5. However, the nature of the CDW that results in many novel charge modulations is still under hot debate. Based on the first-principles calculations, we discover two kinds of CDW states in AV_3Sb_5, namely, the trimerized-hexamerized 2×2 phase and the dimerized 4×1 phase. Our phonon spectrum and electronic Lindhard function calculations reveal that the most intensive structural instability in AV_3Sb_5 originates from a combined in-plane vibration mode of V atoms through the electron-phonon coupling, rather than the Fermi surface nesting effect. More importantly, a metastable 4×1 phase with the V-V dimer pattern and twofold symmetric bow-tie-shaped charge modulation is revealed in CsV_3Sb_5. Further analyses demonstrate that both the in-plane phonon instability and c direction interaction play important roles during the 4×1 phase formation, which provides key understanding for the mechanism of the 4×1 CDW and relative novel phenomena in CsV_3Sb_5.

DOI: 10.1103/PhysRevB.105.245121

I. INTRODUCTION

Kagome materials are a unique platform to study topological physics [1], flat bands [2], geometrical spin frustration [3], and their interactions. In the beginning, large band gap kagome magnets were widely studied as a promising quantum spin liquid system [4–8]. Encouraged by the quantum anomalous Hall (QAH) effect initially proposed for the ferromagnetic kagome material $Cs_2LiMn_3F_{12}$ [1], the topological physics [9–11], electronic correlated flat bands [2,12], and quantum transport induced by the nontrivial Berry curvature [13,14] in kagome metals have attracted increasing interest. Additionally, the interplay between electronic correlation, magnetic frustration, and topology usually gives rise to a variety of intriguing quantum phenomena [15], including the fractional QAH effect [16], topological phase transition [17], spin or charge density waves (SDWs or CDWs) [18,19], and superconductivity [20–22]. Recently, a new family of quasi-two-dimensional (quasi-2D) kagome metals AV_3Sb_5 (A = K, Rb, Cs) was synthesized [23] and was reported to host topological bands [24], unconventional superconductivity [25,26], Van Hove singularities (VHSs), and CDW [27–31], which provides a natural platform to study the interplay among these quantum states.

The pristine AV_3Sb_5 compounds share the same layered structure satisfying space group $P6/mmm$ (No. 191), where A atoms at the $1a$ (0, 0, 0) site form the triangle lattice, V atoms at the $3g$ ($\frac{1}{2}$, 0, $\frac{1}{2}$) site form a kagome layer, Sb1 atoms at $1b$ (0, 0, $\frac{1}{2}$) occupy the center of the V hexagon, and Sb2 atoms at $4h$ ($\frac{1}{3}$, $\frac{2}{3}$, z) form two honeycomb layers. These materials undergo a CDW transition while cooling down to about 80–100 K [25,27,28] and enter the superconducting phase with T_c = 0.9–2.5 K [25,26,32]. For the CDW phase, a 2×2 or $2\times2\times2$ superlattice with trimerization and hexamerization of V atoms (referred to as a T&H phase) was discovered in KV_3Sb_5 [27] and CsV_3Sb_5 [29,33]. An additional 4×1 CDW phase was further observed by scanning tunneling microscopy (STM) experiments in CsV_3Sb_5 when the samples were cooled down to 50 K [34–37]. Some theoretical and experimental works suggested that the CDW might originate from the electron correlation [19,38–47]. Some x-ray scattering and angle-resolved photoemission spectroscopy (ARPES) experiments suggested that it is mainly induced by the Fermi surface (FS) nesting of the VHS at the M points [48]. One calculation study attributed the driving force of CDWs to the Jahn-Teller effect [49]. Very recently, more and more calculations, ARPES, and neutron scattering experiments have proposed that the 2×2 CDW phase in AV_3Sb_5 is driven by the phonon instability through the electron-phonon coupling (EPC) [50–59]. For the 4×1 CDW, Zhao *et al.* proposed that it may be associated with the bulk electronic nematicity [36,37], while Li *et al.* attributed it to the surface instability and electron correlation [60]. Therefore, the nature of the CDW and its relation to the electronic structures, EPC, electron correlation, and superconductivity remain under hot debate for AV_3Sb_5.

In this paper, we construct a variety of supercells to study the structural instability and charge modulation in AV_3Sb_5 based on the first-principles calculations. Our calculations reveal that the most stable structure in AV_3Sb_5 is the 2×2 T&H phase. Further phonon spectrum and Lindhard function calculations demonstrate that such CDW instability is mainly driven by a combined in-plane vibration mode of V atoms, rather than the FS nesting effect. Such a vibration gives rise

*gangxu@hust.edu.cn

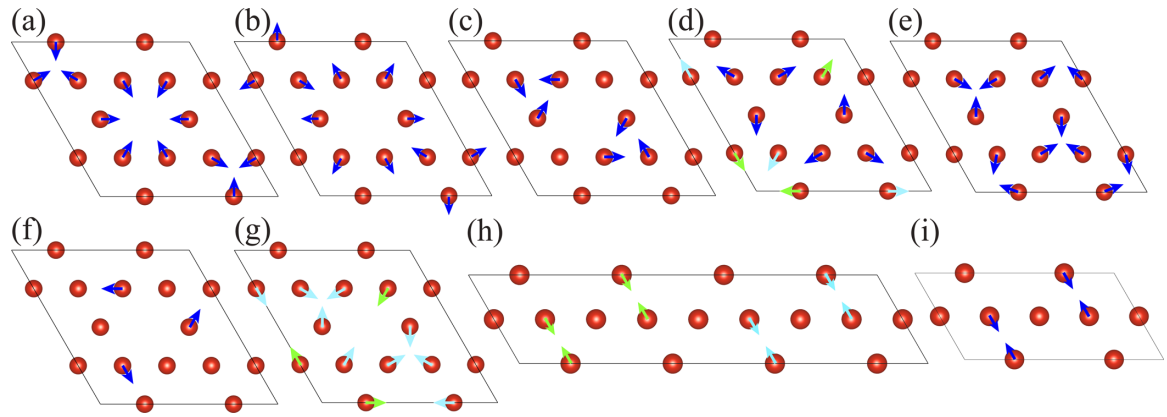

FIG. 1. The top view of V atom movements. (a)–(g) are the 2×2 supercells satisfying (a) and (b) D_{6h} (T&H and SD, respectively), (c) C_{6h}, (d) D_{3d}, (e) D_{3h}, (f) C_{3h}, and (g) C_{3v}, while (h) and (i) are the 4×1 Dimer phase and 2×1 Dimer phase, respectively. The blue arrows represent the pure in-plane movements, and the green (cyan) arrows represent the in-plane movements accompanied by a slight upward (downward) shift along the c direction.

to a negative phonon mode at the M point, which can be hardened after the trimerization and hexamerization of V atoms in the T&H phase. More importantly, a metastable 4×1 phase with a V-V dimer pattern is also discovered in CsV_3Sb_5 and originates from a combined effect of the negative $A_g(M_1)$ phonon mode locking and the c direction interaction. A twofold symmetric bow-tie-shaped charge modulation is reported in the 4×1 phase, which can well explain the electronic nematicity [37] and twofold resistivity anisotropy in CsV_3Sb_5 [35]. These results shed light on the understanding of the 4×1 phase and relative novel phenomena in CsV_3Sb_5.

II. CALCULATION METHODS

Our first-principles calculations are carried out using the Vienna Ab-initio Simulation Package (VASP) [61–63]. The generalized gradient approximation of the Perdew-Burke-Ernzerhof type is adopted for the exchange-correlation potential [64]. The cutoff energy for the wave function expansion is set to 500 eV, and a 16×16×9 k mesh is used to sample the first Brillouin zone. The experimental lattice parameters $a = 5.48$ Å, $c = 8.958$ Å (KV_3Sb_5) and $a = 5.44$ Å, $c = 9.33$ Å (CsV_3Sb_5) are used [29], and all structures are optimized until the force on each atom is less than 0.01 eV/Å. The unfolded band structures of CsV_3Sb_5 are obtained from the Wannier functions using WANNIER90 [65] and the WANNIERTOOLS package [66].

III. RESULTS AND DISCUSSION

Considering that many experimental results indicate the time-reversal symmetry breaking in AV_3Sb_5 [24,27,67–71], we study the magnetic instability by calculating many magnetic configurations. However, the energies always return to the nonmagnetic (NM) state (see more details in Fig. 5 and Table III in the Appendix), indicating the absence of magnetism at the density functional theory level. These results are consistent with recent experiments [23,72], implying that the time-reversal symmetry breaking effect may come from many-body effects, including the exotic CDW instability.

According to the above calculations, we will study the structural instability of AV_3Sb_5 based on just the NM calculations for different supercells and structural distortions. First, let us focus on the structural instability of KV_3Sb_5. For this purpose, we construct a 2×2 supercell from the pristine phase and lower its symmetry by adjusting the coordinates of V atoms. As a result, the seven structural configurations shown in Figs. 1(a)–1(g) are obtained. We notice that the T&H phase in Fig. 1(a) and Star of David (SD) phase in Fig. 1(b) both satisfy the point group D_{6h}, and Figs. 1(c)–1(g) satisfy the C_{6h}, D_{3d}, D_{3h}, C_{3h}, and C_{3v} point groups, respectively. To find the most stable structure, all of the above superlattices and the pristine structure of KV_3Sb_5 are optimized. The calculated energies are listed in Table I. It demonstrates that the T&H phase with the shrunk trimers and hexamers of the V atoms is the most stable one, which agrees well with previous experiments and calculations [27,29]. Further analysis shows that, after the optimization, the V atoms in many other structures tend to the same movements as that in the T&H phase. These results indicate that the trimerization and hexamerization of V atoms play important roles in stabilizing the crystal structure in AV_3Sb_5.

Very similar results and conclusions are obtained for the 2×2 superlattice of CsV_3Sb_5 (see more details in Table IV in the Appendix). Therefore, we just select the T&H phase

TABLE I. The energy of KV_3Sb_5 for different structures.

Structure	Energy (eV/f.u.)
Pristine	−50.511
T&H	−50.519
SD	−50.514
C_{6h}	−50.518
D_{3d}	−50.514
D_{3h}	−50.518
C_{3h}	−50.514
C_{3v}	−50.514
4 × 1 Dimer	−50.513
2 × 1 Dimer	−50.513

TABLE II. The energy of CsV_3Sb_5 for different structures.

Structure	Energy (eV/f.u.)	
Pristine	−50.571	
Structure	Energy (eV/f.u.)	
	(2 × 2)	(2 × 2×2)
T&H	−50.586	−50.586
C_{6h}	−50.585	−50.585
D_{3d}	−50.575	−50.575
C_{3v}	−50.575	−50.575
Structure	Energy (eV/f.u.)	
4×1 Dimer	−50.5741	
2×1 Dimer	−50.5727	

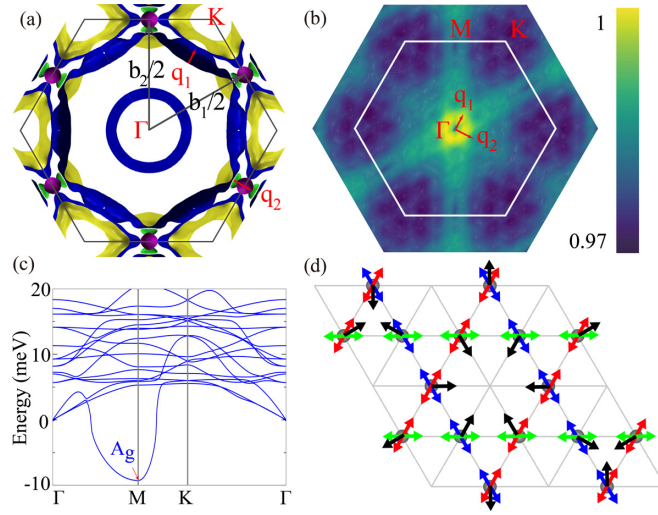

FIG. 2. (a) The top view of the FSs of KV_3Sb_5 along the (001) direction. Two red arrows represent two small nesting vectors, $\vec{q}_1$ and $\vec{q}_2$. (b) Normalized 2D Lindhard response function $\chi_0(q)$ in the b_1-b_2 plane. (c) The phonon spectrum of pristine CsV_3Sb_5. (d) The A_g vibration modes of V atoms at three M points, where the gray circles represent the V atoms, and the blue, green, and red arrows represent the vibration at the M_1 $(\pi, 0, 0)$, M_2 $(0, \pi, 0)$, and M_3 $(\pi, \pi, 0)$ points, respectively. The black arrows denote the combined vibrations for each V atom.

and C_{6h}, D_{3d}, and C_{3v} types of structures as representatives and list their results in Table II. Furthermore, starting from the 2×2 structures, we also construct the corresponding 2×2×2 structural configurations by modulating the V atoms along the c direction. The calculated energies of the optimized 2×2×2 structures are the same as those of the corresponding 2×2 structures, as shown in Table II. Therefore, we conclude that the primary driven force for the 2×2 or 2×2×2 CDW in AV_3Sb_5 mainly comes from the in-plane instability.

More importantly, a metastable 4×1 phase, accompanied by the V-V in-plane dimer movements and slight c direction shifts, as shown in Fig. 1(h), is also discovered for the bulk and film calculations of CsV_3Sb_5, which corresponds to the recent experimental observations very well [34–36]. As shown in II, the energy of such a 4×1 supercell is 3 meV/f.u. lower than that of the pristine phase and 12 meV/f.u. higher than that of the T&H phase. Moreover, the 2×1 supercell with pure in-plane V atom movements shown in Fig. 1(i) is constructed and optimized. The calculated energy of the 2×1 phase with pure in-plane V-V dimers is 1.4 meV/f.u. higher than that in the 4×1 phase with tiny c direction shifts. In addition, we also perform the calculations for the 4×1 phase and 2×1 phase in KV_3Sb_5, although they have not been reported in the experiment. The calculated results as listed in Table I demonstrate that both the 4×1 phase and 2×1 phase in KV_3Sb_5 are 2.0 meV/f.u. lower than its pristine structure. These results reveal that, besides the in-plane V-V dimer instability, some tiny c direction interaction, which is absent in KV_3Sb_5, plays a crucial role during the 4×1 phase formation in CsV_3Sb_5.

To check whether the CDW instability originates from the FS nesting and the Peierls instability as pointed out by the recent x-ray scattering and ARPES experiments [48,73], we calculate the FSs of the pristine KV_3Sb_5 and plot the top view in Fig. 2(a). The FSs of KV_3Sb_5 have quasi-2D characteristics with a columnar FS around the Γ center, while other triprismatic FSs surround the K point. As a result, the FSs do not show any overlap when shifting them by the vector $\vec{b}_1/2$ or $\vec{b}_2/2$, and only a weak FS nesting effect can be induced by shifting two small vectors, $\vec{q}_1$ and $\vec{q}_2$, as shown in Fig. 2(a). The Lindhard response function $\chi_0(q)$ is straightforward evidence of the FS nesting instability [74]. The real part $\chi'(q)$ and imaginary part $\chi''(q)$ of the Lindhard response function $\chi_0(q)$ are solved as follows [38]:

$$\chi'(q) = \sum_k \frac{f(\epsilon_k) - f(\epsilon_{k+q})}{\epsilon_k - \epsilon_{k+q}}, \tag{1}$$

$$\lim_{\omega\to\infty} \chi''(q,\omega)/\omega = \sum_k \delta(\epsilon_k - \epsilon_F)\delta(\epsilon_{k+q} - \epsilon_F). \tag{2}$$

We calculate the 2D renormalized $\chi_0(q)$ of KV_3Sb_5 and plot it in Fig. 2(b). Obviously, no peaks of $\chi_0(q)$ appear at the nesting vectors $\vec{b}_1/2$ and $\vec{b}_2/2$ that correspond to the 2×2 supercell. Figure 2(b) just exhibits some weak peaks at small $\vec{q}$, i.e., $\vec{q}_1$ and $\vec{q}_2$ in Fig. 2(a). These results strongly demonstrate that the CDW instability in AV_3Sb_5 is not from the FS nesting effect.

Next, we focus our attention on the phonon spectrum of AV_3Sb_5 and display the results for CsV_3Sb_5 to study the structural instability induced by EPC. The calculated phonon spectrum of pristine CsV_3Sb_5 is plotted in Fig. 2(c). As reported in Ref. [48], no phonon anomaly appears at the Γ point. However, an optical softening phonon with A_g representation is observed at the $M_1(\pi, 0, 0)$ point in Fig. 2(c), which corresponds to the vibration of V atoms along the (010) direction as illustrated by the blue arrows in Fig. 2(d). Furthermore, the A_g modes at the other two M points, i.e., $M_2(0, \pi, 0)$ and $M_3(\pi, \pi, 0)$, give rise to the vibration of V atoms along the (100) and (110) directions, respectively. Combining the A_g modes at the three M points, the total vibration modes are consistent with movements of V atoms in the T&H or SD phase. To strengthen such a softening mode, one natural manner is to shorten the distance between V atoms, which occurs in the T&H phase [see the black arrows in Fig. 2(d)]. Thus, our results demonstrate that the EPC plays a crucial role

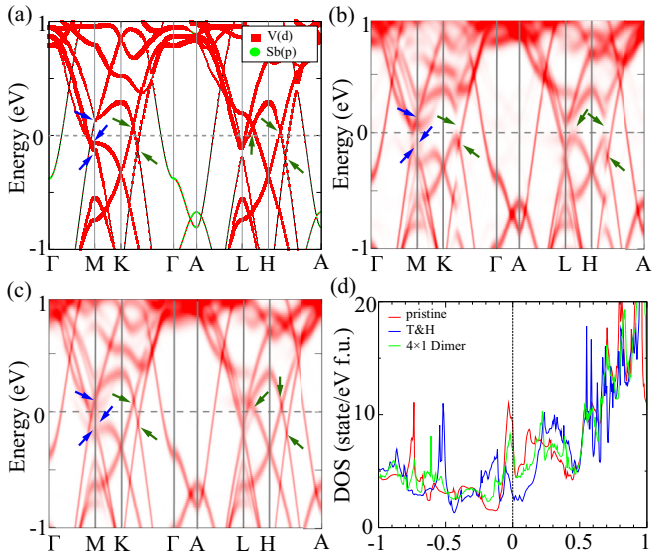

FIG. 3. (a) The projected band structures of pristine CsV_3Sb_5. (b) and (c) The unfolded band structures of the 2×2 T&H phase and 4×1 Dimer phase, respectively. The blue and dark green arrows indicate VHS points and Dirac points, respectively. (d) The DOS of CsV_3Sb_5 in the pristine phase (red), 2×2 T&H phase (blue), and 4×1 Dimer phase (green).

in the formation of the 2×2 or 2×2×2 CDW phase in AV_3Sb_5, which is very consistent with a very recent neutron scattering experiment [52].

For the metastable 4×1 phase, only the negative A_g mode at the $M_1(\pi, 0, 0)$ point should be folded into the Γ point, which could give rise to a V-V dimer similar to those shown in Figs. 1(h) and 1(i) by locking the corresponding vibrations. Such a physical picture agrees well with the finding in Ref. [37] that the 4×1 phase is related to the bulk electronic nematicity. However, we should point out that the $A_g(M_1)$ mode locking can lead to only the 2×1 phase without c direction shifts, as shown in Fig. 1(i), rather than the 4×1 phase shown in Fig. 1(h). These results indicate that both the c direction interaction and in-plane dimer instability originating from the $A_g(M_1)$ mode play crucial roles in stabilizing the 4×1 phase, which is consistent with our energy comparison between the 2×1 and 4×1 phases.

In the following, we discuss the changes in the electronic properties between different structural phases. In Fig. 3(a), we plot the projected band structure of pristine CsV_3Sb_5. Consistent with a previous report [23], there are many VHS points and Dirac points close to the Fermi level, resulting in a relatively high density of states (DOS) at the Fermi level [$N_{E_f} = 8.92$ state/(eV f.u.)]. After the 2×2 reconstruction, most of the VHS points and Dirac points are gapped, as shown in Fig. 3(b), which leads to a DOS transformation from the Fermi level to the higher or lower energy. We notice that nonzero Berry curvature is usually associated with the gapped Dirac points [75], which may be the reason for the observed anomalous Hall effect [24,68]. In the metastable 4×1 Dimer phase, only the spectral weight contributed by the VHS points at the M point is weakened, while the Dirac points are marginally affected, as shown in Fig. 3(c). So weak

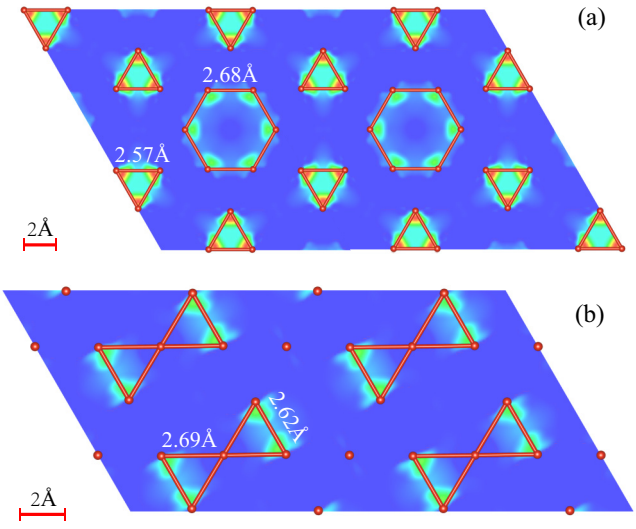

FIG. 4. (a) and (b) The differential charge density distribution in the V kagome layer of CsV_3Sb_5 in the 2×2 T&H phase and 4×1 Dimer phase, respectively.

DOS suppression is observed. We summarize the change in the DOS in Fig. 3(d), which demonstrates that the 2×2 and 4×1 reconstructions lead to different DOS suppressions at the Fermi level and give rise to $N_{E_f} = 2.84$ state/(eV f.u.) for the 2×2 T&H phase and $N_{E_f} = 6.93$ state/(eV f.u.) for the 4×1 Dimer phase.

Finally, we calculate the differential charge density distribution of the 2×2 T&H and 4×1 Dimer CsV_3Sb_5, i.e., the real-space charge difference between the CDW phase and pristine phase, which reveals the real-space charge modulation directly and can be compared with the STM observations qualitatively. The differential charge density distribution in the V kagome layer is plotted in Fig. 4. In the 2×2 T&H phase, the bonds of V trimers (2.57 Å) and hexamers (2.68 Å) are shorter than those of the pristine kagome lattice (2.72 Å). Particularly, Fig. 4(a) illustrates that the charge density in the V trimers is higher than that in the V hexamers, indicating a stronger charge assembling effect in the trimer, which agrees well with previous experimental and theoretical results [30]. On the other hand, the charge density modulation in the 4×1

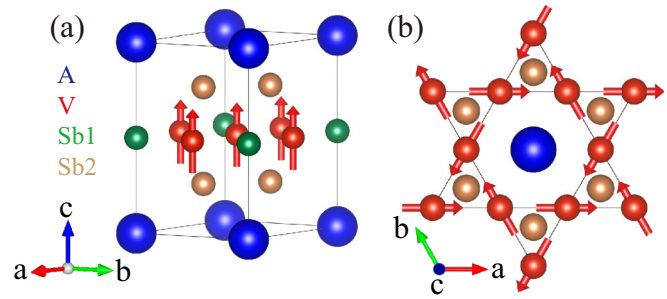

FIG. 5. (a) The crystal structure of AV_3Sb_5 with the FM configuration. (b) Top view along the hexagonal c axis to show the V kagome layer with the 120°-AFM configuration. The red arrows represent the magnetic moment direction of V atoms.

TABLE III. The energy of pristine KV_3Sb_5 for different magnetic configurations. The magnetic moment (MagMom) with/without spin-orbit coupling (SOC) are listed.

	Without SOC		With SOC	
State	Energy (eV)	MagMom (μ_B)	Energy (eV)	MagMom (μ_B)
NM	−50.511	0.00	−50.837	0.00
FM	−50.511	0.00	−50.837	0.00
120°-AFM	−50.511	0.00	−50.837	0.00

Dimer phase is quite different from that in the 2×2 T&H phase. As illustrated in Fig. 4(b), the V atoms in the 4×1 Dimer phase tend to form the V-V dimers along the (010) direction with a bond length of 2.62 Å. These results indicate that competition between dimerization and trimerization may exist in CsV_3Sb_5. More importantly, a twofold-symmetric bow-tie-shaped charge accumulation emerges, as shown in Fig. 4(b). Such charge modulation may be responsible for the twofold resistivity anisotropy in CsV_3Sb_5 [35]. Last, we would like to note that the charge modulation in the 4×1 phase is somewhat weaker than that in the 2×2 T&H phase, which is consistent with the analysis of their electronic structures in Fig. 3.

IV. SUMMARY

In summary, our results indicate that both the 2×2 and 4×1 CDWs originate from the phonon instability instead of the FS nesting effect. The most stable 2×2 T&H phase can be obtained by locking the combined in-plane vibration of V atoms to eliminate all negative A_g phonon modes at three M points. This conclusion agrees well with many of the latest experimental observations [29,30,70]. More importantly, a metastable 4×1 phase with a V-V dimer and bow-tie-shaped charge modulation is discovered in CsV_3Sb_5. Our calculations demonstrated that, besides the in-plane dimer instability induced by the A_g mode at the M_1 (π, 0, 0) point, the c direction interaction plays a crucial role in stabilizing the 4×1 phase rather than the 2×1 phase. These results provide key understanding of the mechanism of the 4×1 phase and relative novel phenomena in CsV_3Sb_5, such as the electronic nematicity [37] and twofold resistivity anisotropy [35].

TABLE IV. The energy of CsV_3Sb_5 for different structures.

Structure	Energy (eV/f.u.)	
Pristine	−50.571	
Structure	Energy (eV/f.u.)	
	(2×2)	(2×2×2)
T&H	−50.586	−50.586
SD	−50.575	−50.575
C_{6h}	−50.585	−50.585
D_{3d}	−50.575	−50.575
D_{3h}	−50.585	−50.585
C_{3h}	−50.575	−50.575
C_{3v}	−50.575	−50.575

ACKNOWLEDGMENTS

We thank P. Dai, B. Yan, and J. Zhao for valuable discussions. This work is supported by the National Key Research and Development Program of China (Grant No. 2018YFA0307000) and the National Natural Science Foundation of China (Grant No. 11874022). Work at Princeton University is supported by the Gordon and Betty Moore Foundation (Grants No. GBMF4547 and No. GBMF9461).

APPENDIX

Considering that much experimental evidence of time-reversal symmetry (TRS) breaking has been reported for AV_3Sb_5 [24,27,67–71], we carry out a series of calculations for the ferromagnetic (FM) configuration [Fig. 5(a)] and in-plane antiferromagnetic configuration with a 120° angle (120°-AFM) [Fig. 5(b)] to study their magnetic instability. Since the results for KV_3Sb_5 and CsV_3Sb_5 are the same, we just list the calculated results for KV_3Sb_5 in Table III, which demonstrates that the FM and AFM configurations always return to the nonmagnetic (NM) state and their energies are the same as that of the NM state. These results are consistent with recent experiments [23,72], which reported that KV_3Sb_5 is a paramagnetic material. Our results imply that these TRS breaking effects may come from the charge density wave transition or the correlation effect. In Table IV, we calculate the energy of seven structural configurations as well as 2×2×2 supercell for CsV_3Sb_5. These results are similar to KV_3Sb_5.

[1] G. Xu, B. Lian, and S.-C. Zhang, Intrinsic Quantum Anomalous Hall Effect in the Kagome Lattice $Cs_2LiMn_3F_{12}$, Phys. Rev. Lett. **115**, 186802 (2015).

[2] J.-X. Yin, S. S. Zhang, G. Chang, Q. Wang, S. S. Tsirkin, Z. Guguchia, B. Lian, H. Zhou, K. Jiang, I. Belopolski, N. Shumiya, D. Multer, M. Litskevich, T. A. Cochran, H. Lin, Z. Wang, T. Neupert, S. Jia, H. Lei, and M. Z. Hasan, Negative flat band magnetism in a spin-orbit-coupled correlated kagome magnet, Nat. Phys. **15**, 443 (2019).

[3] M. R. Norman, Colloquium: Herbertsmithite and the search for the quantum spin liquid, Rev. Mod. Phys. **88**, 041002 (2016).

[4] A. Olariu, P. Mendels, F. Bert, F. Duc, J. C. Trombe, M. A. de Vries, and A. Harrison, ^{17}ONMR Study of the Intrinsic Magnetic Susceptibility and Spin Dynamics of the Quantum Kagome Antiferromagnet $ZnCu_3(OH)_6Cl_2$, Phys. Rev. Lett. **100**, 087202 (2008).

[5] L. Balents, Spin liquids in frustrated magnets, Nature (London) **464**, 199 (2010).

[6] S. Yan, D. A. Huse, and S. R. White, Spin-liquid ground state of the S = 1/2 kagome Heisenberg antiferromagnet, Science **332**, 1173 (2011).

[7] T.-H. Han, J. S. Helton, S. Chu, D. G. Nocera, J. A. Rodriguez-Rivera, C. Broholm, and Y. S. Lee, Fractionalized excitations

in the spin-liquid state of a kagome-lattice antiferromagnet, Nature (London) **492**, 406 (2012).

[8] Y. Shen, Y.-D. Li, H. Wo, Y. Li, S. Shen, B. Pan, Q. Wang, H. Walker, P. Steffens, M. Boehm, Y. Hao, D. L. Quintero-Castro, L. W. Harriger, M. D. Frontzek, L. Hao, S. Meng, Q. Zhang, G. Chen, and J. Zhao, Evidence for a spinon Fermi surface in a triangular-lattice quantum-spin-liquid candidate, Nature (London) **540**, 559 (2016).

[9] L. Ye, M. Kang, J. Liu, F. Von Cube, C. R. Wicker, T. Suzuki, C. Jozwiak, A. Bostwick, E. Rotenberg, D. C. Bell, L. Fu, R. Comin, and J. G. Checkelsky, Massive Dirac fermions in a ferromagnetic kagome metal, Nature (London) **555**, 638 (2018).

[10] J.-X. Yin *et al.*, Quantum-limit Chern topological magnetism in $TbMn_6Sn_6$, Nature (London) **583**, 533 (2020).

[11] H. Tsai, T. Higo, K. Kondou, T. Nomoto, A. Sakai, A. Kobayashi, T. Nakano, K. Yakushiji, R. Arita, S. Miwa, Y. Otani, and S. Nakatsuji, Electrical manipulation of a topological antiferromagnetic state, Nature (London) **580**, 608 (2020).

[12] M. Kang *et al.*, Dirac fermions and flat bands in the ideal kagome metal FeSn, Nat. Mater. **19**, 163 (2020).

[13] S. Nakatsuji, N. Kiyohara, and T. Higo, Large anomalous Hall effect in a non-collinear antiferromagnet at room temperature, Nature (London) **527**, 212 (2015).

[14] E. Liu *et al.*, Giant anomalous Hall effect in a ferromagnetic kagome-lattice semimetal, Nat. Phys. **14**, 1125 (2018).

[15] J.-X. Yin *et al.*, Giant and anisotropic many-body spin–orbit tunability in a strongly correlated kagome magnet, Nature (London) **562**, 91 (2018).

[16] E. Tang, J.-W. Mei, and X.-G. Wen, High-Temperature Fractional Quantum Hall States, Phys. Rev. Lett. **106**, 236802 (2011).

[17] Z. He, A. Luo, B. Lian, and G. Xu, Interplay of topological electrons and magnons in the kagome magnet $CoCu_3(OH)_6Cl_2$, New J. Phys. **23**, 113007 (2021).

[18] S.-L. Yu and J.-X. Li, Chiral superconducting phase and chiral spin-density-wave phase in a Hubbard model on the kagome lattice, Phys. Rev. B **85**, 144402 (2012).

[19] W.-S. Wang, Z.-Z. Li, Y.-Y. Xiang, and Q.-H. Wang, Competing electronic orders on kagome lattices at Van Hove filling, Phys. Rev. B **87**, 115135 (2013).

[20] M. L. Kiesel and R. Thomale, Sublattice interference in the kagome Hubbard model, Phys. Rev. B **86**, 121105(R) (2012).

[21] M. L. Kiesel, C. Platt, and R. Thomale, Unconventional Fermi surface instabilities in the kagome Hubbard model, Phys. Rev. Lett. **110**, 126405 (2013).

[22] C. Mielke, Y. Qin, J.-X. Yin, H. Nakamura, D. Das, K. Guo, R. Khasanov, J. Chang, Z. Q. Wang, S. Jia, S. Nakatsuji, A. Amato, H. Luetkens, G. Xu, M. Z. Hasan, and Z. Guguchia, Nodeless kagome superconductivity in $LaRu_3Si_2$, Phys. Rev. Materials **5**, 034803 (2021).

[23] B. R. Ortiz, L. C. Gomes, J. R. Morey, M. Winiarski, M. Bordelon, J. S. Mangum, I. W. H. Oswald, J. A. Rodriguez-Rivera, J. R. Neilson, S. D. Wilson, E. Ertekin, T. M. McQueen, and E. S. Toberer, New kagome prototype materials: Discovery of KV_3Sb_5, RbV_3Sb_5, and CsV_3Sb_5, Phys. Rev. Materials **3**, 094407 (2019).

[24] S.-Y. Yang, Y. Wang, B. R. Ortiz, D. Liu, J. Gayles, E. Derunova, R. Gonzalez-Hernandez, L. Šmejkal, Y. Chen, S. S. P. Parkin, S. D. Wilson, E. S. Toberer, T. McQueen, and M. N. Ali, Giant, unconventional anomalous Hall effect in the metallic frustrated magnet candidate, KV_3Sb_5, Sci. Adv. **6**, eabb6003 (2020).

[25] B. R. Ortiz, S. M. L. Teicher, Y. Hu, J. L. Zuo, P. M. Sarte, E. C. Schueller, A. M. Milinda Abeykoon, M. J. Krogstad, S. Rosenkranz, R. Osborn, R. Seshadri, L. Balents, J. He, and S. D. Wilson, CsV_3Sb_5: A $\mathbb{Z}_2$ Topological Kagome Metal with a Superconducting Ground State, Phys. Rev. Lett. **125**, 247002 (2020).

[26] Y. Wang, S. Yang, P. K. Sivakumar, B. R. Ortiz, S. M. L. Teicher, H. Wu, A. K. Srivastava, C. Garg, D. Liu, S. S. P. Parkin, E. S. Toberer, T. McQueen, S. D. Wilson, and M. N. Ali, Proximity-induced spin-triplet superconductivity and edge supercurrent in the topological kagome metal, $K_{1-x}V_3Sb_5$, arXiv:2012.05898

[27] Y.-X. Jiang *et al.*, Unconventional chiral charge order in kagome superconductor KV_3Sb_5, Nat. Mater. **20**, 1353 (2021).

[28] Q. Yin, Z. Tu, C. Gong, Y. Fu, S. Yan, and H. Lei, Superconductivity and normal-state properties of kagome metal RbV_3Sb_5 single crystals, Chin. Phys. Lett. **38**, 037403 (2021).

[29] H. Tan, Y. Liu, Z. Wang, and B. Yan, Charge Density Waves and Electronic Properties of Superconducting Kagome Metals, Phys. Rev. Lett. **127**, 046401 (2021).

[30] X. Feng, K. Jiang, Z. Wang, and J. Hu, Chiral flux phase in the kagome superconductor AV_3Sb_5, Sci. Bull. **66**, 1384 (2021).

[31] J. Zhao, W. Wu, Y. Wang, and S. A. Yang, Electronic correlations in the normal state of the kagome superconductor KV_3Sb_5, Phys. Rev. B **103**, L241117 (2021).

[32] B. R. Ortiz, P. M. Sarte, E. M. Kenney, M. J. Graf, S. M. L. Teicher, R. Seshadri, and S. D. Wilson, Superconductivity in the $\mathbb{Z}_2$ kagome metal KV_3Sb_5, Phys. Rev. Materials **5**, 034801 (2021).

[33] Z. Liang, X. Hou, F. Zhang, W. Ma, P. Wu, Z. Zhang, F. Yu, J.-J. Ying, K. Jiang, L. Shan, Z. Wang, and X.-H. Chen, Three-Dimensional Charge Density Wave and Surface-Dependent Vortex-Core States in a Kagome Superconductor CsV_3Sb_5, Phys. Rev. X **11**, 031026 (2021).

[34] Z. Wang *et al.*, Electronic nature of chiral charge order in the kagome superconductor CsV_3Sb_5, Phys. Rev. B **104**, 075148 (2021).

[35] H. Chen *et al.*, Roton pair density wave in a strong-coupling kagome superconductor, Nature (London) **599**, 222 (2021).

[36] H. Zhao, H. Li, B. R. Ortiz, S. M. L. Teicher, T. Park, M. Ye, Z. Wang, L. Balents, S. D. Wilson, and I. Zeljkovic, Cascade of correlated electron states in a kagome superconductor CsV_3Sb_5, Nature (London) **599**, 216 (2021).

[37] L. Nie *et al.*, Charge-density-wave-driven electronic nematicity in a kagome superconductor, Nature (London) **604**, 59 (2022).

[38] M. D. Johannes and I. I. Mazin, Fermi surface nesting and the origin of charge density waves in metals, Phys. Rev. B **77**, 165135 (2008).

[39] S. Barišić, J. Labbé, and J. Friedel, Tight Binding and Transition-Metal Superconductivity, Phys. Rev. Lett. **25**, 919 (1970).

[40] F. Weber, S. Rosenkranz, J.-P. Castellan, R. Osborn, R. Hott, R. Heid, K.-P. Bohnen, T. Egami, A. H. Said, and D. Reznik, Extended Phonon Collapse and the Origin of the Charge-Density Wave in $2H$-$NbSe_2$, Phys. Rev. Lett. **107**, 107403 (2011).

[41] X. Zhu, Y. Cao, J. Zhang, E. W. Plummer, and J. Guo, Classification of charge density waves based on their nature, Proc. Natl. Acad. Sci. USA **112**, 2367 (2015).

[42] J.-P. Pouget, E. Canadell, and B. Guster, Momentum-dependent electron-phonon coupling in charge density wave systems, Phys. Rev. B **103**, 115135 (2021).

[43] C. M. Varma and A. L. Simons, Strong-Coupling Theory of Charge-Density-Wave Transitions, Phys. Rev. Lett. **51**, 138 (1983).

[44] M. H. Christensen, T. Birol, B. M. Andersen, and R. M. Fernandes, Theory of the charge density wave in AV_3Sb_5 kagome metals, Phys. Rev. B **104**, 214513 (2021).

[45] J. Zaanen and O. Gunnarsson, Charged magnetic domain lines and the magnetism of high-T_c oxides, Phys. Rev. B **40**, 7391 (1989).

[46] K. Machida, Magnetism in La_2CuO_4 based compounds, Phys. C (Amsterdam, Neth.) **158**, 192 (1989).

[47] D. Poilblanc and T. M. Rice, Charged solitons in the Hartree-Fock approximation to the large-U Hubbard model, Phys. Rev. B **39**, 9749 (1989).

[48] H. Li, T. T. Zhang, T. Yilmaz, Y. Y. Pai, C. E. Marvinney, A. Said, Q. W. Yin, C. S. Gong, Z. J. Tu, E. Vescovo, C. S. Nelson, R. G. Moore, S. Murakami, H. C. Lei, H. N. Lee, B. J. Lawrie, and H. Miao, Observation of Unconventional Charge Density Wave without Acoustic Phonon Anomaly in Kagome Superconductors AV_3Sb_5 (A = Rb, Cs), Phys. Rev. X **11**, 031050 (2021).

[49] C. Wang, S. Liu, H. Jeon, and J.-H. Cho, Origin of charge density wave in the layered kagome metal CsV_3Sb_5, Phys. Rev. B **105**, 045135 (2022).

[50] H. Luo, Q. Gao, H. Liu, Y. Gu, D. Wu, C. Yi, J. Jia, S. Wu, X. Luo, Y. Xu, L. Zhao, Q. Wang, H. Mao, G. Liu, Z. Zhu, Y. Shi, K. Jiang, J. Hu, Z. Xu, and X. J. Zhou, Electronic nature of charge density wave and electron-phonon coupling in kagome superconductor KV_3Sb_5, Nat. Commun. **13**, 273 (2022).

[51] S. Cho, H. Ma, W. Xia, Y. Yang, Z. Liu, Z. Huang, Z. Jiang, X. Lu, J. Liu, Z. Liu, J. Jia, Y. Guo, J. Liu, and D. Shen, Emergence of New Van Hove Singularities in the Charge Density Wave State of a Topological Kagome Metal RbV_3Sb_5, Phys. Rev. Lett. **127**, 236401 (2021).

[52] Y. Xie, Y. Li, P. Bourges, A. Ivanov, Z. Ye, J.-X. Yin, M. Z. Hasan, A. Luo, Y. Yao, Z. Wang, G. Xu, and P. Dai, Electron-phonon coupling in the charge density wave state of CsV_3Sb_5, Phys. Rev. B **105**, L140501 (2022).

[53] H. Miao, H. X. Li, W. R. Meier, A. Huon, H. N. Lee, A. Said, H. C. Lei, B. R. Ortiz, S. D. Wilson, J. X. Yin, M. Z. Hasan, Z. Wang, H. Tan, and B. Yan, Geometry of the charge density wave in the kagome metal AV_3Sb_5, Phys. Rev. B **104**, 195132 (2021).

[54] T. Qian, M. H. Christensen, C. Hu, A. Saha, B. M. Andersen, R. M. Fernandes, T. Birol, and N. Ni, Revealing the competition between charge density wave and superconductivity in CsV_3Sb_5 through uniaxial strain, Phys. Rev. B **104**, 144506 (2021).

[55] J.-F. Zhang, K. Liu, and Z.-Y. Lu, First-principles study of the double-dome superconductivity in the kagome material CsV_3Sb_5 under pressure, Phys. Rev. B **104**, 195130 (2021).

[56] A. Ptok, A. Kobiałka, M. Sternik, J. Łażewski, P. T. Jochym, A. M. Oleś, and P. Piekarz, Dynamical study of the origin of the charge density wave in AV_3Sb_5 (A = K, Rb, Cs) compounds, arXiv:2110.09816.

[57] A. Subedi, Hexagonal-to-base-centered-orthorhombic $4q$ charge density wave order in kagome metals KV_3Sb_5, RbV_3Sb_5, and CsV_3Sb_5, Phys. Rev. Materials **6**, 015001 (2022).

[58] Z. Wang, S. Ma, Y. Zhang, H. Yang, Z. Zhao, Y. Ou, Y. Zhu, S. Ni, Z. Lu, H. Chen, K. Jiang, L. Yu, Y. Zhang, X. Dong, J. Hu, H.-J. Gao, and Z. Zhao, Distinctive momentum dependent charge-density-wave gap observed in CsV_3Sb_5 superconductor with topological kagome lattice, arXiv:2104.05556.

[59] K. Nakayama, Y. Li, T. Kato, M. Liu, Z. Wang, T. Takahashi, Y. Yao, and T. Sato, Multiple energy scales and anisotropic energy gap in the charge-density-wave phase of the kagome superconductor CsV_3Sb_5, Phys. Rev. B **104**, L161112 (2021).

[60] H. Li, Y.-X. Jiang, J. X. Yin, S. Yoon, A. R. Lupini, Y. Pai, C. Nelson, A. Said, Y. M. Yang, Q. W. Yin, C. S. Gong, Z. J. Tu, H. C. Lei, B. Yan, Z. Wang, M. Z. Hasan, H. N. Lee, and H. Miao, Spatial symmetry constraint of charge-ordered kagome superconductor CsV_3Sb_5, arXiv:2109.03418.

[61] G. Kresse and J. Furthmüller, Efficient iterative schemes for *ab initio* total-energy calculations using a plane-wave basis set, Phys. Rev. B **54**, 11169 (1996).

[62] G. Kresse and J. Hafner, *Ab initio* molecular dynamics for open-shell transition metals, Phys. Rev. B **48**, 13115 (1993).

[63] G. Kresse and D. Joubert, From ultrasoft pseudopotentials to the projector augmented-wave method, Phys. Rev. B **59**, 1758 (1999).

[64] J. P. Perdew, K. Burke, and M. Ernzerhof, Generalized Gradient Approximation Made Simple, Phys. Rev. Lett. **77**, 3865 (1996).

[65] A. A. Mostofi, J. R. Yates, G. Pizzi, Y.-S. Lee, I. Souza, D. Vanderbilt, and N. Marzari, An updated version of wannier90: A tool for obtaining maximally-localised Wannier functions, Comput. Phys. Commun. **185**, 2309 (2014).

[66] Q. Wu, S. Zhang, H.-F. Song, M. Troyer, and A. A. Soluyanov, Wanniertools: An open-source software package for novel topological materials, Comput. Phys. Commun. **224**, 405 (2018).

[67] D. W. Song, L. X. Zheng, F. H. Yu, J. Li, L. P. Nie, M. Shan, D. Zhao, S. J. Li, B. L. Kang, Z. M. Wu, Y. B. Zhou, K. L. Sun, K. Liu, X. G. Luo, Z. Y. Wang, J. J. Ying, X. G. Wan, T. Wu, and X. H. Chen, Orbital ordering and fluctuations in a kagome superconductor CsV_3Sb_5, arXiv:2104.09173.

[68] F. H. Yu, T. Wu, Z. Y. Wang, B. Lei, W. Z. Zhuo, J. J. Ying, and X. H. Chen, Concurrence of anomalous Hall effect and charge density wave in a superconducting topological kagome metal, Phys. Rev. B **104**, L041103 (2021).

[69] C. M. III *et al.*, Time-reversal symmetry-breaking charge order in a correlated kagome superconductor, Nature **602**, 245 (2022).

[70] L. Yu, C. Wang, Y. Zhang, M. Sander, S. Ni, Z. Lu, S. Ma, Z. Wang, Z. Zhao, H. Chen, K. Jiang, Y. Zhang, H. Yang, F. Zhou, X. Dong, S. L. Johnson, M. J. Graf, J. Hu, H.-J. Gao, and Z. Zhao, Evidence of a hidden flux phase in the topological kagome metal CsV_3Sb_5, arXiv:2107.10714.

[71] N. Shumiya, M. S. Hossain, J.-X. Yin, Y.-X. Jiang, B. R. Ortiz, H. Liu, Y. Shi, Q. Yin, H. Lei, S. S. Zhang, G. Chang, Q. Zhang, T. A. Cochran, D. Multer, M. Litskevich, Z.-J. Cheng, X. P. Yang, Z. Guguchia, S. D. Wilson, and M. Z. Hasan, Intrinsic nature of chiral charge order in the kagome superconductor RbV_3Sb_5, Phys. Rev. B **104**, 035131 (2021).

[72] E. M. Kenney, B. R. Ortiz, C. Wang, S. D. Wilson, and M. Graf, Absence of local moments in the kagome metal KV_3Sb_5

as determined by muon spin spectroscopy, J. Phys.: Condens. Matter **33**, 235801 (2021).

[73] B. R. Ortiz, S. M. L. Teicher, L. Kautzsch, P. M. Sarte, N. Ratcliff, J. Harter, J. P. C. Ruff, R. Seshadri, and S. D. Wilson, Fermi Surface Mapping and the Nature of Charge-Density-Wave Order in the Kagome Superconductor CsV_3Sb_5, Phys. Rev. X **11**, 041030 (2021).

[74] D. Wu, Q. M. Liu, S. L. Chen, G. Y. Zhong, J. Su, L. Y. Shi, L. Tong, G. Xu, P. Gao, and N. L. Wang, Layered semiconductor $EuTe_4$ with charge density wave order in square tellurium sheets, Phys. Rev. Materials **3**, 024002 (2019).

[75] M. Perrot, P. Delplace, and A. Venaille, Topological transition in stratified fluids, Nat. Phys. **15**, 781 (2019).